Conclusions

Analytical design equations (26) and (27) were derived for leaky membranes ($\theta \neq 0$). These equations show a substantial improvement over the analytical design equations of Gupta (1985) and Sirkar and Rao (1982) which are valid for high rejection membranes. The iterative procedure required in the solution of $(\bar{X}_{23})^+$ from eq 27 may be avoided by using simplified design equations (26) and (41). Even simpler design equations (26) and (44) may be obtained for large η. It is shown that the design equations (26) and (41) provide fairly accurate results for all values of η, and the design equations (26) and (44) may be used for $\eta \geq 1$.

Acknowledgment

We acknowledge the support and suggestions of Dr. D. M. Misra, BARC.

Nomenclature

A = pure water permeability constant, g-mol/(cm^2·s·atm)
b = constant defined as $b = \pi(C_{2j})/C_{2j}$ for $j = 2$ and 3
B = parameter defined in eq 40
C = total molar density of solution, g-mol/cm^3
C_{sj} = concentration of species at location j; $s = 1$ for solvent; $s = 2$ for solute; $j = 1$ for feed stream; $j = 2$ for high pressure side membrane; $j = 3$ for permeate stream, g-mol/cm^2
D_{2m} = diffusivity of solute in membrane phase, cm^2/s
$D_{2m}/K\delta$ = solute transport parameter treated as a single quantity, cm/s
$E_1(u)$ = exponential integral = $\int_u^\infty \exp(-u)/u\ du$
Ei(ω) = exponential integral = $\int_w^\infty \exp(w)/w\ dw$
$1/h$ = membrane surface area per unit volume of feed channel, cm^{-1}
k = mass-transfer coefficient on high-pressure side, cm/s
K = ratio of solute concentration in solution over solute concentration in membrane with which the solution is in contact
L = length of membrane from channel entrance, cm
L^+ = dimensionless length of membrane = αL
N_1 = solvent flux at location x, g-mol/(cm^2·s)
N_2 = solute flux at location x, g-mol·cm^2·s
ΔP = applied pressure difference across membrane at location x, atm
$\bar{v}_x$ = bulk velocity of solution on high-pressure side at any x, cm/s
V = dimensionless velocity = $\bar{v}_x/\bar{v}_{xf}$
x = axial distance from channel entrance, cm
X = dimensionless distance = αx
X_{21}, X_{22}, X_{23} = solute mole fractions in feed stream, high-pressure-side membrane solution interface, and permeate solution at any x
X_{11} = solvent mole fraction at any x
X_{21}^+, X_{22}^+, X_{23}^+ = normalized solute mole fraction of feed steam, high-pressure-side membrane solution interface, and permeate stream at any $x = X_{2j}/X_{21f}$
u = dimensionless variable = $\gamma Z/\eta V$
w = dimensionless variable = $(1/\eta) - u$
u_1, w_1 = values of u and w at the channel entrance
u_2, w_2 = values of u and w at any location x
Z = concentration polarization = $(X_{22} - X_{23})/(X_{21} - X_{23})$
Z_1 = concentration polarization at the entrance
Z_2 = concentration polarization at any x

Greek Letters

α = parameter = $A\Delta P/(Ch\bar{v}_{xf})$, cm^{-1}
π = osmotic pressure of solute in the solution of concentration C_{2j}, atm
γ = dimensionless osmotic pressure = $bCX_{21f}/\Delta P$
γ' = $\gamma[1 - (\bar{X}_{23})^+]$
Δ = fractional solvent recovery = $1 - V$
θ = dimensionless solute permeability = $(D_{2m}/K\delta)/(A\Delta P/C)$
η = dimensionless mass-transfer coefficient = $k/(A\Delta P/C)$
δ = effective membrane thickness

Subscripts

f = refers to high-pressure-side feed at channel entrance
$j = 1$ = feed stream, 2 = high-pressure-side wall, 3 = permeate steam
0 = refers to the values for high rejection membranes
1, 2 = refers to the conditions at the entrance and at any location x

Superscripts

– = refers to average value over the module

Literature Cited

Gupta, S. K. *Ind. Eng. Chem. Process Des. Dev.* **1985**, *24*(4), 1240.
Handbook of Mathematical Functions; Abramowitz, M., Stegun, I. A., Eds.; Bureau of Standards: Washington, DC, 1968; Applied Mathematics Series, Vol. 55; p 238.
Ohya, H.; Sourirajan, S. *Reverse Osmosis System Specification and Performance Data for Water Treatment*; Thyer School of Engineering, Dartmouth College: Hanover, NH, 1971.
Sirkar, K. K.; Rao, G. H. *Ind. Eng. Chem. Process Des. Dev.* **1982**, *21*, 517.
Sourirajan, S. *Reverse Osmosis*; Logos: London, 1970.

Received for review September 11, 1985
Accepted May 16, 1986

COMMUNICATIONS

Electrostatic Enhancement of Industrial Drying Processes

We report here results from an energy-efficient electrostatic drying technique which increases the rate of evaporation from a variety of materials. The method works by using a moderately strong, heterogeneous electrostatic field to create turbulence near a wet surface, thereby disrupting the surface boundary layer of inert gas and increasing the rate at which molecules of water or other liquids can diffuse away. This process may have industrial applications and may be particularly useful in situations which require low air velocities or for materials which cannot be dried by using conventional techniques.

Although the process of drying consumes a substantial fraction of the energy used in many manufacturing processes, the basic techniques presently in use have remained unchanged for many decades (e.g.: Keey, 1978). Most of

0196-4305/86/1125-1027$01.50/0

these involve blowing heated air over the wet material, heating the substrate upon which the material is drying, and using infrared or microwave radiation to heat the water or other liquids directly, or various combination of these things. Most of these drying techniques serve the dual purpose of increasing the heat transferred to the evaporating liquid and enhancing the removal of the moisture-laden air.

It is well-known from the study of transport phenomena that a thin layer of relatively inert air exists at the surface of most materials where the relative velocity of gas flow asymptotically drops to zero. These surface boundary layers both interfere with the diffusion of gases out of the material and limit the rate of convective heat transfer into it (e.g.: Burke, 1932; Bird et al., 1960; Choi, 1968). Both of these effects limit the rate of drying, and it is clear that a simple method disrupting this layer might improve the energy efficiency of many drying processes.

It is also known that a sharp, electrically conducting point will produce an electric or "corona" wind as a result of ions leaving the point, and this wind can cause a marked increase in heat conduction at a surface by disrupting the insulating surface boundary layer (Allen et al., 1959; Lykoudis and Yu, 1963; Kronig and Schwartz, 1947; Cobine, 1973; Robinson, 1970; Bonjour et al., 1962). This effect has been used to increase the cooling rate of hot surfaces during welding, to cool semiconductor elements, and to cool optical components in CO_2 lasers (Cobine, 1973).

Despite the fact that these surface boundary layers are known to inhibit both the processes of heat transfer and drying, techniques used to increase the rate of heat transfer are not commonly used in drying processes; this is particularly true with respect to electrostatic enhancement. Electrostatics are not mentioned in either of Keey's (1972, 1978) two major volumes on industrial drying processes nor are they mentioned in the volume on the industrial applications of electrostatics edited by Moore (1973); this is surprising, particularly because several patents have been issued within the US on related topics (e.g.: Dairah, 1936; Candor, 1984). In this paper we therefore explore the possibility that electrostatic disruption of this boundary layer might also lead to an increased rate of drying and note that it should be an energy-efficient process because the effects are produced with extremely low current flow.

We report here a series of electrostatic drying rate experiments along with initial measurements of the overall energy efficiency of this process. Our results confirm the predictions and earlier reports discussed above and suggest that electrostatic enhancement could be used in conjunction with a variety of commercially used industrial drying processes to reduce their energy consumption. These conclusions are in agreement with the recent report by Rounsley (1984) who found drying rate improvements of 10–30% even in the presence of forced convection.

Experimental Procedures, Materials, and Methods

We measured the rate of drying under a variety of conditions with the experimental setup shown in Figure 1. Material for each drying experiment was placed on a flat conducting metal plate mounted on a digital centigram balance, and a microcomputer was used to read and store the total weight of the assembly at 10-s intervals. In order to generate the corona discharge needed to form an ion wind, we used an open mesh electrode with sharp needle points suspended 5 cm over the sample assembly and charged with either direct or alternating high voltage. Electric current flowing in the system was measured by connecting the metal sample plate to ground through a 250-Ω resistor and monitoring the voltage drop across it. Heat was supplied to the sample either by a hot-water bath mounted beneath the plate or through an infrared lamp mounted above the upper electrode.

Each experiment began by wetting the material to be dried with 10 g of water and placing it on the balance assembly. For each material, electric field setting, and heat source to be tested, we ran control experiments with no electric field before and after. Initial tests dealt with filter paper, wool, and chopped onions and used four electric field settings (0, 5, 10, and 15 kV or 0, 1, 2, and 3 kV/cm).

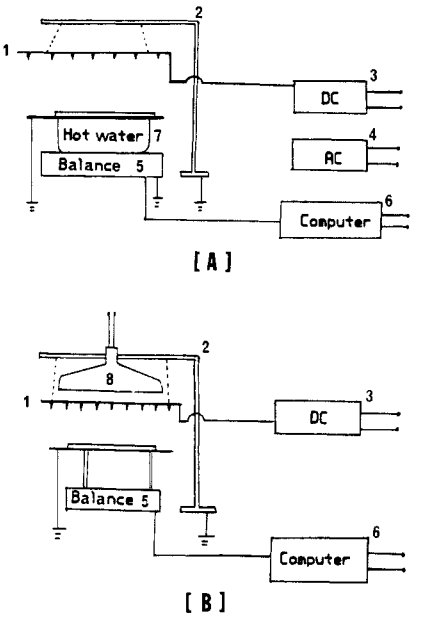

Figure 1. Experimental setup for measuring the rate of drying under various applied electrostatic fields. (A) illustrates the method of appling heat to the evaporating liquid through a hot-water bath, while (B) shows the setup for heating the drying surface with an infrared light. Small numbers on each diagram are as follows: The needle point electrodes (1) are suspended by insulators from the support brace (2) and connected to either a high-voltage dc power supply (3) or a high-voltage ac supply (4). The digital centigram balance (5, Mettler Model PE 1600) was read at 10-s intervals by the microcomputer (6, an Apple II+), and heat was applied either through a hot-water bath (7) or through a 500-W infrared lamp (8). Examples of the data generated with these setups are shown in Figure 2.

Table I. Typical Current and Power Requirements for the Electrostatic Drying Experiments Immediately after Starting[a]

appl voltage, kV	polarity	water mass on paper, g	high-voltage current, A	electrostatic power consumption, W
5	−	dry	1.26	0.0063
5	−	10	0.31	0.0015
5	+	10	0.02	0.0001
10	−	dry	29.0	0.296
10	−	10	22.5	0.225
10	+	10	11.0	0.110
15	−	dry	102.0	1.5
15	−	10	94.0	1.4
15	+	10	60.0	0.9

[a] Positive polarity for the voltage means that the electrode is charged positively relative to the substrate (vice versa for negative polarity). For all experiments the electrode was positioned 5 cm above the substrate, and all data reported here used the standard, 15-cm-diameter filter paper. Current flowing through the high-voltage circuit was measured by monitoring the voltage drop across a 250-Ω resistor connected between the substrate and ground. The power estimate is simply the high-voltage times the current.

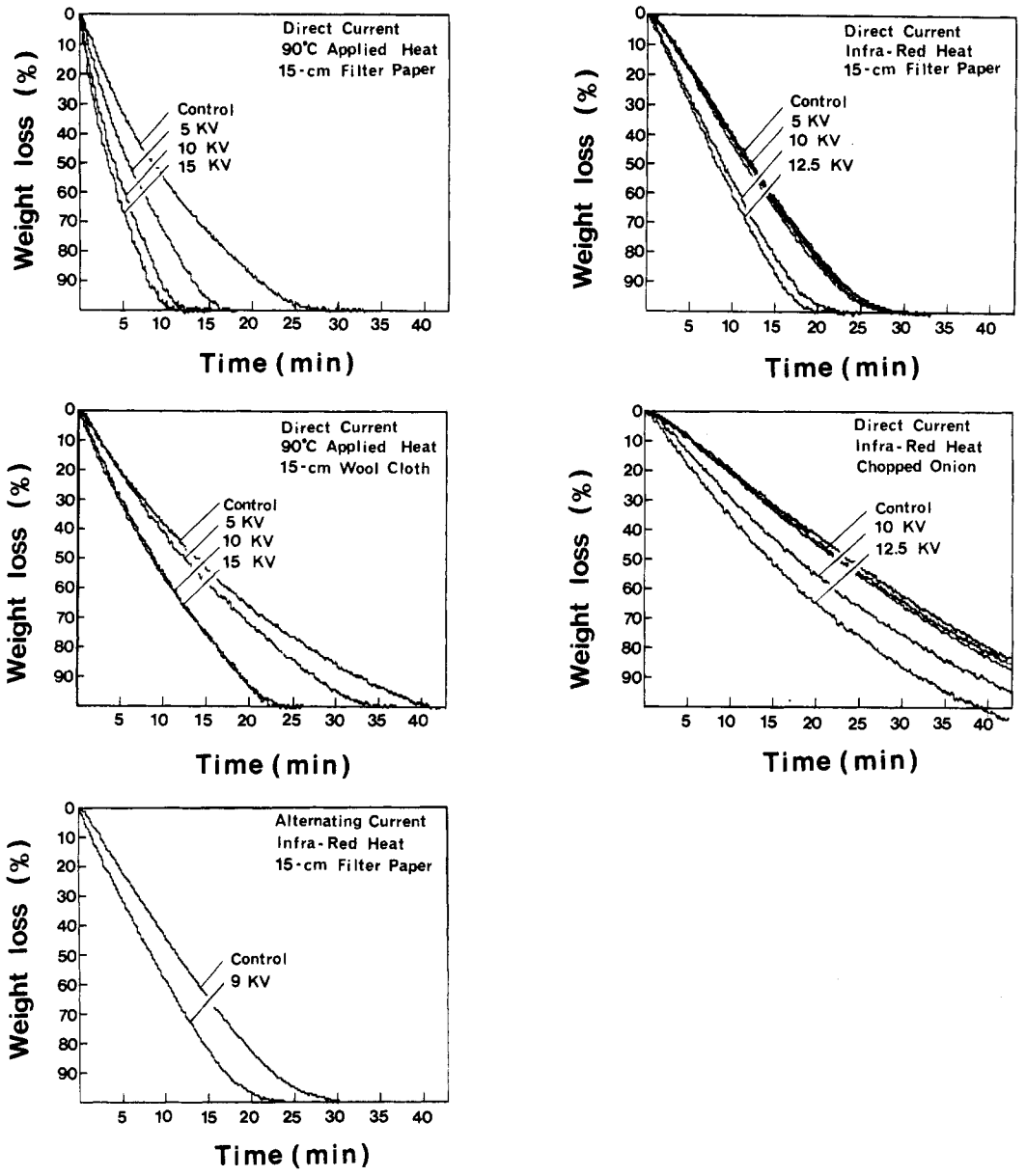

Figure 2. Experimental results from typical drying rate experiments described in the text and performed with the apparatus shown in Figure 1. Each diagram shown plots the weight loss measured directly from the balance as a function of time from the beginning of the experiment. Data shown on each graph were obtained on the same day, and they were only accepted for days on which there was no measured change in relative humidity or temperature within the lab. Control experiments were performed in precisely the same fashion as those with varying electric fields, except that no voltage was applied.

Results

Figure 2 shows the results of these experiments, and Tables I and II show the measured current flow and calculated power consumption for representative runs using the standard 15-cm-diameter (0.2-mm thick) filter paper with 10 g of water. We found that in most cases the application of electric fields in the 5–15-kV range (1–3 kV/cm) increased the drying rate by between 20% and 50% over that of the controls (depending upon the relative humidity on the particular day). The effect was substantially better when using the direct current (dc) of either polarity than with the alternating current (ac), although all were distinctly faster than the control experiments which did not use the electrostatic enhancement. The drying rate increased rapidly with electric field strength up to about 10 kV and in most cases increased only marginally above that, implying that the optimum efficiency was achieved in the neighborhood of 10 kV, or 2 kV/cm. The additional power applied to the system through the electric field was on the order of 1% of that applied either through the infrared lamp or through the hot-water bath. We obtained similar results using a variety of materials, including but not limited to paper, wool (0.5-mm thick), and chopped onions (average thickness ~2 mm).

Table II. Typical Current and Power Consumption Using Alternating Current Rather than Direct Current

appl alternating voltage, kV	water mass on paper, g	high-voltage current, A	electrostatic power consumption, W
5.6	10	15.0	0.09
5.6	dry	71.0	0.39
7.0	10	20.0	0.14
7.0	dry	91.0	0.64
9.0	10	40.0	3.55
9.0	dry	115.0	1.04

To visualize some of the air turbulence generated by various electric fields, we replaced the lower plate with a

metal grill and allowed a small stream of smoke from a cigarette to flow up between the electrodes. We observed a gradual breakup of the smoke stream with increasing voltage up to between 8 and 10 kV followed by little, if any, increase with the application of stronger field values.

It is interesting to note from Figure 2 that the thickest materials dried (onions and wool) demonstrate the smallest fractional change in drying rate with applied field. In these materials the drying rate is probably influenced more by the diffusion of liquid to the surface than by the inhibiting effect of the surface boundary layer.

Conclusions

(1) The application of a moderately strong heterogeneous electric field to the surface of a drying material significantly enhances the rate of drying.

(2) This effect is probably due to the disruption of the surface boundary layer of inert air which otherwise impedes both diffusion of evaporating molecules from the surface and heat transfer into it.

(3) If applied properly, this technique could yield a large increase in the overall energy efficiency of the drying processes.

Acknowledgment

This work was partially supported by NSF Grant EAR83-51370. This paper is Caltech Division of Geological and Planetary Sciences Contribution No. 4303.

Literature Cited

Allen P. H. G. *Br. J. Appl. Phys.* **1959**, *10*, 347-351.
Bird, R. B.; Stewart, W. E.; Lightfoot, E. N. *Transport Phenomena*.; Wiley: New York, 1960.
Bonjour, E.; Verdier, J.; Weil, L. *Chem. Eng. Prog.* **1962**, *58*, 63-66.
Burke, S. P. U.S. Patent 1 835 557, 1932.
Candor, J. T. U.S. Patent 4 467 529, 1984.
Choi, H. Y., Jr. *Trans. ASME* **1968**, 98-102.
Cobine, J. D. In *Electrostatics and its Applications*; Moore, A. D., Ed.; Wiley: New York, 1973; pp 441-455.
Dairah, W. A. US Patent 2 042 145, 1936.
Keey, R. B. *Drying Principles and Practice*; Pergamon: New York, 1972.
Keey, R. B. *Introduction to Industrial Drying Operations*; Pergamon: New York, 1978.
Kronig, R.; Schwarz, N. *Appl. Sci. Res.* **1947**, *A1*, 35-46.
Lykoudis, P. S.; Yu, C. P. *Int. J. Heat Mass Transfer* **1963**, *6*, 853-862.
Electrostatics and Its Applications; Moore, A. D., Ed.; Wiley: New York, 1973; p 481.
Robinson, M. *Int. J. Heat Mass Transfer* **1970**, *13*, 263-274.
Rounsley, R. R. *Eng. Conf.*, [*Proc.*] **1984**, 341-346.

Division of Geological and Planetary Sciences
The California Institute of Technology
Pasadena, California 91125

Atsuko Kirschvink-Kobayashi*
Joseph L. Kirschvink

Received for review March 8, 1985
Revised manuscript received February 3, 1986
Accepted March 24, 1986

Determination of Volumetric Properties for Systems Containing Structure I Gas Hydrates

A model is developed for determining the volumetric properties of systems containing oxygen, nitrogen, and other Structure I gas hydrates. It uses traditional statistical thermodynamics to determine the hydrate number (N_i) and defines the extent of hydration (ξ) which represents the relative amount of gas that enters into the hydrate phase. The molar volumes of the systems at the saturated hydrate and saturated H_2O (liquid or solid) limits can then be expressed in terms of ξ. These molar volumes are useful for designing gas-storage vessels in which gas hydrates form.

Using the statistical thermodynamic model developed by van der Waals and Platteeuw (1959), much of the recent research in gas hydrates, a type of crystalline inclusion compound, has been devoted to the prediction of conditions leading to hydrate formation (Holder et al., 1980; Holder and Hand, 1982; Holder and Manganiello, 1982; Holder et al., 1984). Since hydrates can be responsible for fouling gas lines, these conditions must be estimated accurately so that hydrate formation can be prevented. In addition, some hydrocarbon hydrates occur naturally (e.g., methane hydrates in cold climates and on ocean floors) and may become useful sources of natural gas. However, hydrates are also of industrial interest for other reasons such as desalination (Knox et al., 1961), gas separation, and gas storage (Miller and Strong, 1946). This work is intended to quantify the changes that occur in the volume of a gas i upon the formation of a hydrate phase and is, thus, oriented toward the use of hydrates as a means of storing gases. The model presented here can be used to design gas-storage vessels which, being able to withstand the pressures corresponding to hydrate formation, can contain a smaller volume of gas i if i is in the hydrate state rather than in the gaseous state.

Analysis and Discussion

According to X-ray diffraction studies by von Stackelburg and Müller (1954), gas hydrates can be categorized by their structures, the two most common of which are the Structure I and Structure II hydrates. Oxygen and nitrogen, in addition to other gases whose molecular diameters are on the order of 0.5 nm or less, form primarily Structure I hydrates. This type of hydrate is comprised of two pentagonal dodecahedral (σ) cavities and six tetrakaidecahedral (λ) cavities per unit cell. Inherently unstable, these crystalline cavities can exist only when they are occupied by gas molecules which are held in the lattices by van der Waals forces. However, evidence presented by van Cleef and Diepen (1965) and Gallaway et al. (1970) has shown that the degree of occupation of these guest molecules in the cavities is less than 100%. This can be seen by considering the empirical formula of a Structure I hydrate, given by $G_i \cdot N_i H_2O$ where G_i is the hydrate-forming molecule and N_i is the nonstoichiometric hydrate number. The hydrate number is defined as in eq 1 where

$$N_i = \frac{46}{2\theta_{\sigma i} + 6\theta_{\lambda i}} \quad (1)$$

0196-4305/86/1125-1030$01.50/0